JOURNAL OF AGRICULTURAL AND FOOD CHEMISTRY

Effect of Xanthan on the Molecular Mobility of Amorphous Sucrose Detected by Erythrosin B Phosphorescence

YUMIN YOU AND RICHARD D. LUDESCHER*

Department of Food Science, Rutgers, The State University of New Jersey, 65 Dudley Road, New Brunswick New Jersey 08901-8520

Molecular mobility in amorphous solids is modulated by composition and environmental conditions such as temperature. Phosphorescence of erythrosin B was used to generate a mobility map of amorphous sucrose film doped with xanthan gum at weight ratios of xanthan/sucrose ranging from 0.0001 to 0.01. On the basis of analysis of the emission energy and lifetime of erythrosin B in pure sucrose and sucrose−xanthan films over the temperature range from 5 to 100 °C, we conclude that xanthan influences the molecular mobility as well as the dynamic site heterogeneity of amorphous sucrose in a dose-dependent fashion. At xanthan/sucrose weight ratios below ∼0.0005, both emission energy and lifetime decreased and k_{TS0} (the nonradiative decay rate of the triplet state) increased, indicating that xanthan increased the matrix molecular mobility. At weight ratios above 0.001, both emission energy and lifetime increased and k_{TS0} decreased, indicating that xanthan decreased matrix mobility, reaching a plateau at weight ratios between 0.005 and 0.01. The concentration at which the effect of xanthan switched from increasing to decreasing mobility was similar to the concentration at which polymer chains overlapped in solution, suggesting that the dynamic changeover reflected the onset of chain overlap in the amorphous solid. Systematic trends in the emission bandwidth and lifetime heterogeneity and variations in the emission lifetime vs wavelength indicated that xanthan reduced the matrix dynamic site heterogeneity except at a weight ratio of 0.01. These data illustrate the complex effects of a polymer with a rigid structure and large side chains on the mobility of an amorphous, hydrogen-bonded sugar matrix.

KEYWORDS: Amorphous; phosphorescence; molecular mobility; xanthan; sucrose

INTRODUCTION

The properties of amorphous solid sucrose are important for the texture and shelf life of dried and frozen foods (*1*), the long-term stability of pharmaceuticals (*2*), and the ability of plants to survive desiccation and drought (*3*). Two distinct aspects of sucrose have been invoked to explain its importance in stabilizing sensitive compounds during dehydration and storage (*4*). First, sucrose readily forms a rigid, hard, brittle glass upon drying or cooling concentrated aqueous solutions. This rigid matrix provides a relatively inert environment in which the rates of physical change and chemical reaction are slow (*5*). Second, sucrose can form hydrogen bonds at specific sites with target compounds (such as protein surfaces or the hydrophilic head-groups of membrane lipids), bonds which help maintain the native structure and integrity of the molecule or molecular complex after the removal of water (*6*).

Sucrose glasses found in foods and pharmaceutical formulations often include other compounds such as low molecular weight salts and high molecular weight hydrocolloids. The precise mechanisms by which these compounds modulate the properties of the amorphous solid are uncertain. We have recently shown that the addition of sodium chloride to amorphous sucrose causes a dose-dependent decrease in the local molecular mobility of the matrix (*7*). This rigidifying effect seems to be a general property of both inorganic and organic salts (*8*). The effect of gelatin on sucrose matrix mobility is more complex (*9*); gelatin increases matrix mobility at low levels of addition and decreases matrix mobility at high levels.

Most research on sugars and hydrocolloids has focused on how sugars modulate the properties of polysaccharides in aqueous solutions and in solid gels at low to medium sugar levels. Here, we report results from an investigation of the effect of the polysaccharide xanthan on the physical properties of an amorphous sucrose matrix. Xanthan, an anionic polysaccharide that provides very high viscosity and is commonly used as a thickener and stabilizer in food systems, was selected as an example of a nongelling, relatively rigid, high molecular weight polysaccharide.

In previous studies, we have used erythrosin B (Ery B) phosphorescence to monitor the molecular mobility as well as

* To whom correspondence should be addressed. Tel: 732-932-9611ext. 231. Fax: 732-932-6776. E-mail: ludescher@aesop.rutgers.edu.

10.1021/jf802501m CCC: $40.75
Published on Web 12/30/2008

dynamic site heterogeneity in amorphous solid sucrose (*10, 11*), in other amorphous sugars (*12*), and in sucrose−gelatin films (*9*). In the present study, phosphorescence of Ery B was used to monitor the matrix mobility in amorphous films dried from sucrose mixtures containing xanthan at weight ratios ranging from 0.0001 to 0.01 g xanthan/g sucrose. Measurements of the phosphorescence emission maximum and excited-state lifetime provide information about how xanthan modulates the molecular mobility of amorphous sucrose at low levels of macromolecule, thus providing insight into the complex mechanism by which this biopolymer affects the solid matrix.

MATERIALS AND METHODS

Preparation of Sucrose Films. Sucrose was purchased from Sigma-Aldrich (St. Louis, MO) with a minimum purity of 99.5%. Sucrose solutions were treated with activated charcoal prior to use to remove any potentially luminescent impurities as described in Pravinata et al. (*10*). The final concentration of the purified sucrose solution was adjusted to 65−67 wt %, with the concentration confirmed using a refractometer (NSG Precision Cells, Inc., Farmingdale, NY). Before it was spread on slides, the sucrose solution was filtered through a 0.2 μm membrane to remove particulates.

The free acid of Ery B (tetra-iodo fluorescein; Sigma Chemical Co., St. Louis, MO) was dissolved to 10 mM in spectrophotometric grade dimethylformamide (DMF; Aldrich Chemical Co., Milwaukee, WI); an aliquot from this solution was added to the concentrated sucrose to obtain a dye/sucrose mole ratio of 1:10^4. Glassy sucrose films ~10−40 μm thick were prepared on quartz slides as described in You and Ludescher (*7*). The slides were stored against P_2O_5 and Drie-Rite for at least 7 days and checked for crystallization by examination through crossed polarizers in a dissecting microscope (Nikon type 102, Japan) before any phosphorescence measurements.

Preparation of Xanthan−Sucrose Films. Xanthan gum (XR80), a generous gift from Food Ingredient Solutions, LLC (Blauvelt, NY), was used without further treatment. Xanthan solution, prepared in distilled deionized water at a concentration of 1 g/100 mL, was kept at 60 °C for 10 min before mixing with the sucrose solution containing Ery B to obtain solutions with xanthan/sucrose weight ratios of 0.0001, 0.0005, 0.001, 0.002, 0.004, 0.005, and 0.01. Prior to preparing glassy films, sucrose−xanthan solutions were filtered through a 0.2 μm membrane (except for the wt ratio of 0.01, which was too viscous to filter). The procedure to make a glassy xanthan-containing film was the same as the procedure to make a pure sucrose film except for drying films for 10 min instead of 5 min. The prepared dry sucrose films at all xanthan levels were as clear and transparent as pure sucrose films, which suggested that no macroscopic phase separation of xanthan-rich domains occurred.

The water content in amorphous sucrose and sucrose−xanthan films was determined gravimetrically by difference of mass before and after drying for 24 h at 70 °C in an Ephortee (Haake Buchler, Inc.) vacuum oven at 1 kPa. Sample films were scratched from quartz slides and ground into powders in a glovebox containing P_2O_5 and Drie-Rite with a relative humidity less than 5%. Pure sucrose films contained 0.56 ± 0.13 wt % water, while xanthan/sucrose samples contained 0.41 ± 0.01, 0.47 ± 0.09, 0.68 ± 0.25, 0.39 ± 0.01, 0.48 ± 0.16, 0.66 ± 0.06, and 0.72 ± 0.21 wt % water for films with xanthan wt ratios of 0.0001, 0.0005, 0.001, 0.002, 0.004, 0.005, and 0.01, respectively.

Luminescence Measurements. Luminescence measurements were made on a Cary Eclipse Fluorescence spectrophotometer (Varian Instruments, Walnut Creek, CA). Slides were placed on end in a standard fluorescence cuvette, and samples were flushed for a minimum of 15 min with nitrogen gas, which contained less than 1 ppm oxygen to eliminate oxygen quenching. At each target temperature, samples were equilibrated for 1 min/°C increase in temperature (the temperature was controlled using a thermoelectric temperature controller provided by Varian Instruments). The chamber surrounding the cuvette holder was flushed with dry air to reduce moisture condensation during measurements at below ambient temperatures. All of the measurements were made at least in triplicate.

Delayed luminescence emission spectra were collected from 520 to 750 nm (10 nm bandwidth) at 1 nm intervals using excitation at 500 nm (20 nm bandwidth) with an observation window of 5.0 ms and an initial delay time of 0.2 ms to suppress fluorescence coincident with the lamp pulse. An emission spectrum from a sample without probe was subtracted from each spectrum (although background signal was very low).

The energy of the emission maximum (ν_p) and the full width at half-maximum (fwhm) of the emission bands were determined using log-normal line shape function (*13*) to fit both delayed fluorescence and phosphorescence emission bands.

$$I(\nu) = I_0 \exp\left\{-\ln(2)\left(\frac{\ln[1 + 2b(\nu - \nu_p)/\Delta]}{b}\right)^2\right\} \quad (1)$$

In this equation, I_0 is the maximum emission intensity, ν_p is the peak frequency (in cm^{-1}), Δ is a line width parameter, and b is an asymmetry parameter. The bandwidth (fwhm; Γ) was calculated as follows:

$$\Gamma = \Delta\left(\frac{\sinh(b)}{b}\right) \quad (2)$$

For delayed luminescence spectra collected from 520 to 750 nm, a sum of log-normal functions for delayed fluorescence [$I_{df}(\nu)$] and phosphorescence [$I_p(\nu)$] was used to fit the spectra. Each emission band was fit to independent fit parameters.

For the determination of lifetime as a function of temperature, samples were excited at 530 nm (20 nm bandwidth), and emission transients were collected at 680 nm (20 nm bandwidth). Phosphorescence intensity decays were collected over a window of 5 ms with an initial delay of 0.1 ms and time increments of 0.04 ms. Each decay was the average of 20 cycles. Because intensity decays were nonexponential, a stretched exponential, or Kohlrausch−Williams−Watts' decay function, was used to analyze the intensity decay (*10*).

$$I(t) = I_0 \exp[-(t/\tau)^{\beta}] + \text{constant} \quad (3)$$

In this equation, I_0 is the initial amplitude at time zero, τ is the stretched exponential lifetime, and β is the stretching exponent that characterizes the distribution of lifetimes. The use of a stretched exponential model provides a direct measure of the distribution of lifetimes considered appropriate for describing a complex glass possessing a distribution of relaxation times for the dynamic molecular processes. The smaller the β value was, the more nonexponential was the intensity decay and thus the broader the distribution of lifetimes (*14*). The program NFIT (Galveston, TX) was used to fit the intensity decays. Goodness of fit was evaluated by examining R^2 and plots of the modified residuals (defined as the fit intensity minus the measured intensity divided by the square root of the measured intensity). R^2 for all fits ranged from 0.99 to 1.00, and modified residuals plots fluctuated randomly around zero amplitude.

Phosphorescence intensity decays of Ery B as a function of emission wavelength were collected with an excitation wavelength of 530 nm (20 nm bandwidth); the emission wavelength varied from 640 to 720 nm (20 nm bandwidth). Phosphorescence emission lifetimes as a function of excitation wavelength were measured with an emission wavelength of 680 nm (20 nm bandwidth); the excitation wavelength ranged from 490 to 560 nm (20 nm bandwidth). These experiments were performed at 25 °C.

Photophysical Scheme. Our scheme for analysis of the delayed luminescence is essentially identical to the photophysical scheme for Ery B outlined by Duchowicz et al. (*15*). The phosphorescence emission rate (k_P) is the sum of all possible deexcitation rates for the triplet state T_1:

$$1/\tau = k_P = k_{RP} + k_{TS1} + k_{TS0} + k_Q[Q] \quad (4)$$

In this equation, k_{RP} is the rate of radiative emission to the ground-state S_0; for Ery B, k_{RP} is 41 s^{-1} and constant with temperature (*15*); k_{TS1} is the rate of thermally activated reverse intersystem crossing from the triplet state T_1 to the singlet state S_1, which follows Arrhenius behavior:

$$k_{TS1}(T) = k_{TS1}{}^{0} \exp(-\Delta E_{TS}/RT) \quad (5)$$

In this equation, k^0_{TS1} is the maximum rate of intersystem crossing at high temperature, ΔE_{TS} is the energy gap between T_1 and S_1, $R = 8.314$ J K^{-1} mol^{-1}, and T is the temperature in Kelvin. The value of ΔE_{TS} was calculated from the slope of a Van't Hoff plot of the natural logarithm of the ratio of the intensity of delayed fluorescence (I_{DF}) to phosphorescence (I_P):

$$d[\ln(I_{DF}/I_P)]/d(1/T) = -\Delta E_{TS}/R \quad (6)$$

(I_{DF} and I_P are the maximum intensity values determined from analysis of the emission band using eq 1). The value of k_{TS1} at 25 °C was estimated as 88 s^{-1} using $k^0_{TS1} = 3.0 \times 10^7$ s^{-1} and $\Delta E_{TS} = 31.56$ kJ/mol (*10*). The temperature-dependent term k_{TS1} was calculated using $k^0_{TS1} = 3.0 \times 10^7$ s^{-1} for all samples except xanthan−sucrose films with a weight ratio of 0.005 ($k_{TS1}{}^0 = 2.6 \times 10^7$ s^{-1}) and 0.01 ($k_{TS1}{}^0 = 2.5 \times 10^7$ s^{-1}).

In the presence of oxygen, the quenching rate $k_Q[Q]$ is the product of the rate constant for collision k_Q and the oxygen concentration $[O_2]$. Under our experimental conditions, with nitrogen purging, $k_Q[O_2] \approx 0$. One of the nonradiative decay routes involves internal conversion to the ground-state S_0 with rate k_{TS0}, which reflects the rate of collisional quenching of the probe due to both internal and external factors (*16*). In this case, the term k_{TS0} primarily reflects external factors since self-collisional quenching among probe molecules can be neglected within the extremely viscous amorphous solid. The temperature-dependent term k_{TS0} can be easily calculated from the phosphorescence lifetime by rewriting eq 4 as follows:

$$k_{TS0}(T) = \frac{1}{\tau(T)} - k_{RP} - k_{TS1}(T) \quad (7)$$

RESULTS

At a probe/sucrose mole ratio of 1:10^4, each probe is on average surrounded by a matrix shell around 10−11 sucrose molecules thick. At this concentration, Ery B dispersed within the sucrose matrix does not appear to aggregate and thus reports the physical properties of the unperturbed sucrose matrix (*11*).

Delayed Emission Spectra. The delayed emission spectra of Ery B dispersed in amorphous sucrose films with various weight ratios of xanthan/sucrose were collected over the temperature range from 5 to 100 °C (data not shown). All spectra showed the decrease in phosphorescence and the increase in delayed fluorescence intensity with increasing temperature expected in xanthene dyes (*10*). The delayed fluorescence and phosphorescence bands shifted to longer wavelengths at higher temperatures; the peak frequency (ν_p) and bandwidth (Γ) were determined by fitting to a log-normal line shape function (eqs 1 and 2). The frequency and bandwidth for phosphorescence emission are plotted vs temperature in **Figure 1**. The peak frequency for delayed fluorescence exhibited similar behavior (data not shown).

A decrease in the phosphorescence peak frequency, a measure of the average energy of emission, reflects an increase in the extent of dipolar relaxation around the excited triplet state prior to emission (*17*). The peak frequency decreased gradually and approximately linearly at low temperature and much more steeply at higher temperature in all films. The total change in peak frequency ($\Delta\nu_p = \nu_{100\,°C} - \nu_{5\,°C}$) was ~340 cm^{-1} in pure sucrose, increased at a weight ratio of 0.002 xanthan/sucrose to a maximum of ~480 cm^{-1}, and decreased to a constant value of ~370 cm^{-1} at weight ratios above 0.005. The change in peak frequency in all xanthan/sucrose films was larger than that seen in sucrose, indicating an increased extent of dipolar relaxation around the excited triplet state over this temperature range in the presence of xanthan. All of the thermal curves had similar

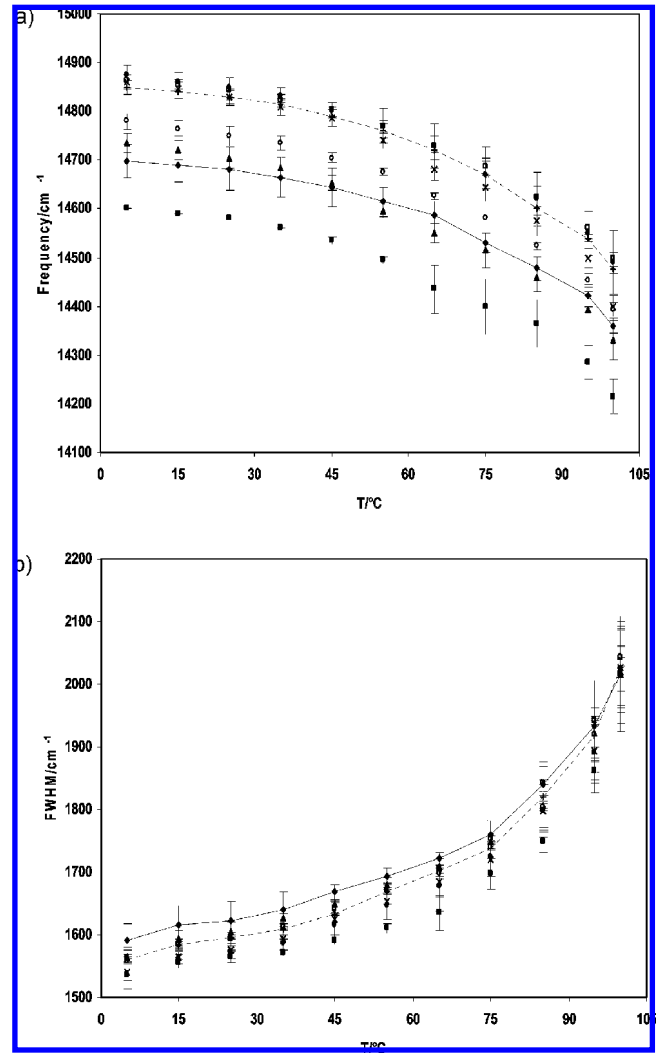

Figure 1. Effect of temperature on the (**a**) peak frequency (ν_p) and (**b**) bandwidth (fwhm) for phosphorescence emission from Ery B dispersed in amorphous sucrose−xanthan films. Delayed emission spectra were analyzed using a log-normal line shape function (see the text for details). Samples are Ery B in sucrose films with the following xanthan/sucrose weight ratios: ♦, 0 (control); ■, 0.0001; ▲, 0.0005; ○, 0.001; ×, 0.002; ●, 0.004; □, 0.005; and +, 0.01.

shapes; however, the curve for the film with a weight ratio of 0.0001 was well below that for sucrose, while curves with weight ratios >0.0005 were above.

The phosphorescence bandwidth provides a measure of the extent of inhomogeneous broadening that the Ery B probe experiences within the amorphous matrix (*17*). The bandwidth increased gradually at low temperature and more dramatically at high temperature in all films. The addition of xanthan slightly decreased the bandwidth over the whole temperature range, with the largest decrease occurring at a weight ratio of 0.0001. The decrease in bandwidth reflects a corresponding decrease in the width of the distribution of energetically distinct matrix environments over the whole temperature range.

The effect of xanthan is demonstrated in plots of peak frequency and bandwidth, normalized to the value in pure sucrose, as a function of xanthan content (**Figure 2**). The peak frequency varied with xanthan content in a complex manner, initially decreasing at a weight ratio 0.0001 and then increasing at a higher xanthan content to a plateau above weight ratio ~0.002. The bandwidth varied with the xanthan content in an even more complicated manner, decreasing significantly at a

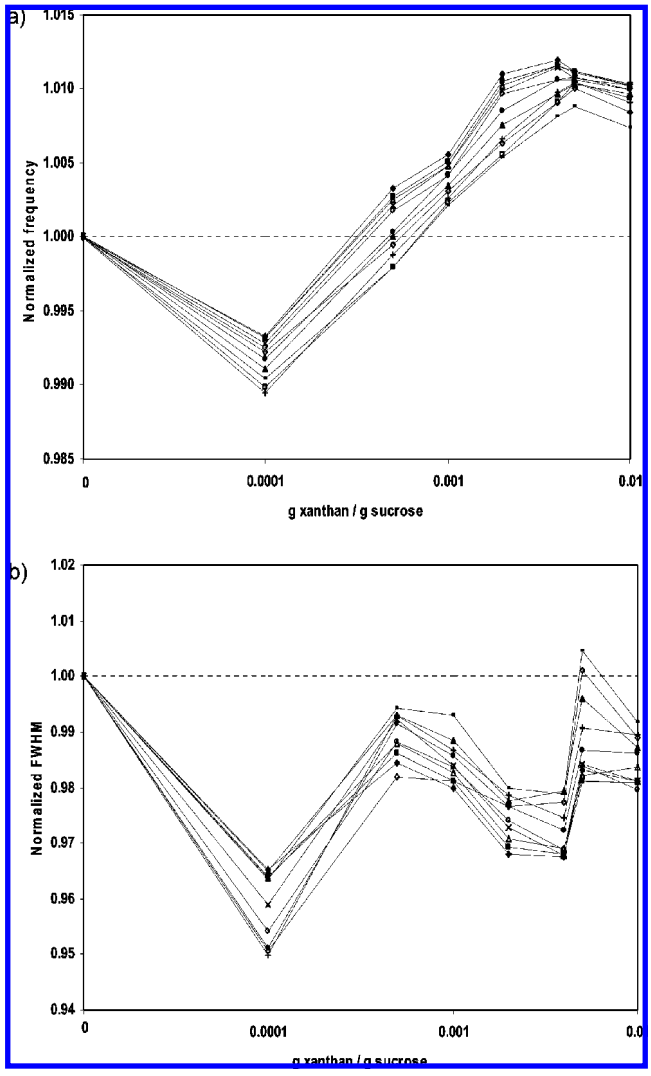

Figure 2. Effect of xanthan content on the phosphorescence (**a**) peak frequency and (**b**) bandwidth (fwhm), normalized at each temperature to the value in pure sucrose, for Ery B dispersed in amorphous sucrose−xanthan films. Data from **Figure 1** are plotted as a function of the weight ratio of xanthan/sucrose at the following temperatures: ♦, 5 °C; ■, 15 °C; △, 25 °C; ×, 35 °C; ○, 45 °C; ●, 55 °C; +, 65 °C; ▲, 75 °C; ◊, 85 °C; −, 95 °C; and □, 100 °C.

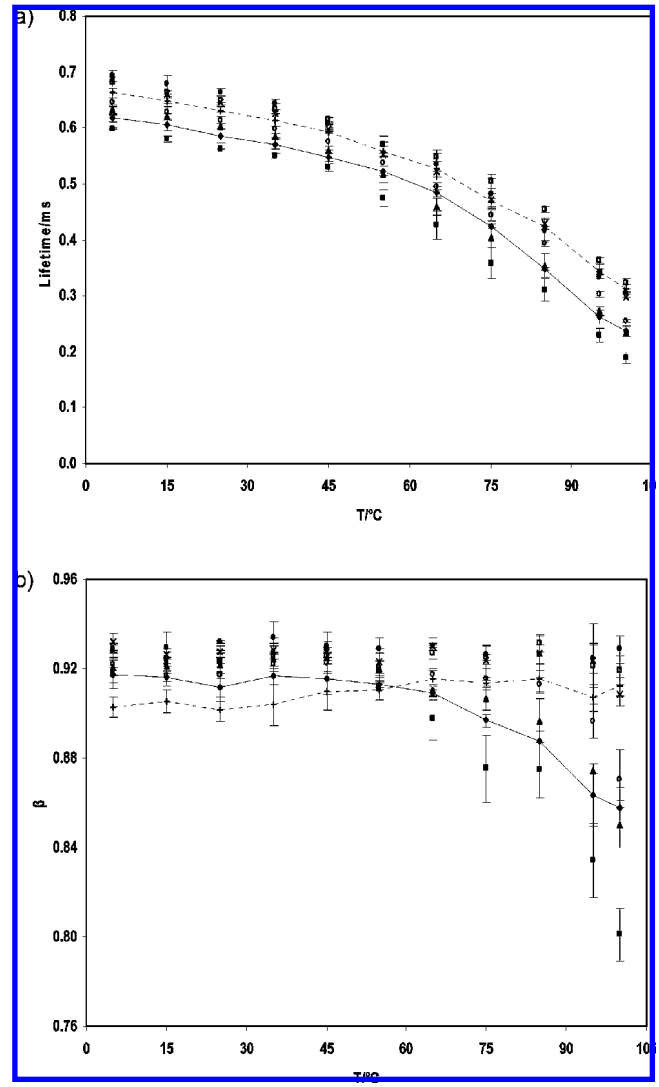

Figure 3. Effect of temperature on the (**a**) lifetime and (**b**) stretching exponent β obtained from fits to a stretched exponential decay model of the intensity decay of Ery B dispersed in amorphous sucrose films. Data are for samples with the following xanthan/sucrose weight ratios: ♦, control, 0; ■, 0.0001; ▲, 0.0005; ○, 0.001; ×, 0.002; ●, 0.004; □, 0.005; and +, 0.01.

0.0001 weight ratio, increasing at 0.0005 to values slightly lower than in sucrose, decreasing again to a minimum at weight ratio of ∼0.004, and increasing again at a weight ratio of 0.005 and above.

The intensity ratio $\ln(I_{DF}/I_P)$ was plotted as a van't Hoff plot vs $1/T$ (data not shown), and the slope obtained from the linear plot was used to estimate the energy gap (ΔE_{TS}) between the triplet and the singlet states (eq 6 in the Materials and Methods). In amorphous sucrose, the value of ΔE_{TS} was 31.56 ± 0.56 kJ mol^{-1}; the values of ΔE_{TS} were 31.92 ± 0.19, 31.32 ± 0.86, 31.64 ± 0.16, 32.12 ± 0.77, 31.13 ± 0.55, 31.32 ± 0.38, and 31.29 ± 0.16 kJ mol^{-1} at weight ratios of 0.0001, 0.0005, 0.001, 0.002, 0.004, 0.005, and 0.01, respectively, indicating that addition of xanthan had no significant effect on the singlet−triplet energy gap.

Phosphorescence Decay Kinetics. The phosphorescence intensity decays of Ery B in sucrose−xanthan glass with different xanthan contents were measured over the temperature range from 5 to 100 °C and fit to a stretched exponential decay function (*10*). The stretched exponential lifetime and stretching exponent β are plotted as a function of temperature in **Figure 3**. The lifetimes decreased biphasically with increasing temperature in all films, exhibiting a gradual linear decrease at low temperature and a more dramatic decrease at high temperature. All of the curves showed similar shapes; however, the lifetimes for films with xanthan/sucrose weight ratio of 0.0001 were below while those with weight ratios >0.0005 were above the lifetimes for pure sucrose. The lifetime generally increased with the addition of xanthan, from 0.63 ms at 5 °C in film with a weight ratio of 0.0005 to 0.69 ms in film with a weight ratio of 0.004; a further increase in xanthan concentration did not increase the lifetime further.

The stretching exponent β exhibited biphasic temperature behavior in sucrose, remaining nearly constant at low temperature and decreasing at ∼65 °C and above. The value of β also decreased at higher temperature at low xanthan weight ratios (0.0001−0.001), but the extent of the decrease varied with xanthan content. At weight ratios of 0.002 and above, however, β was essentially constant with temperature over the full temperature range from 5 to 100 °C. Except at a high weight ratio (0.01) at low temperature and low weight ratio (0.0001)

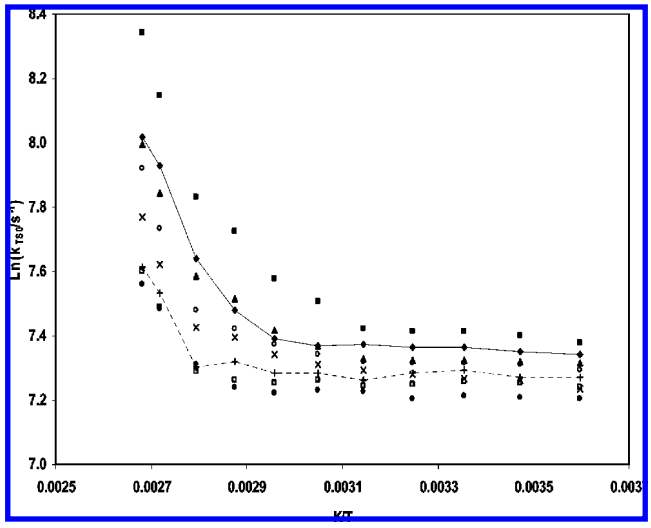

Figure 4. Arrhenius plot of the effect of temperature on the rate constant for nonradiative decay of the triplet T_1 state to S_0 (k_{TS0}); data were calculated from the lifetime data of **Figure 3a** (see the text for additional details). Ery B in amorphous sucrose films with the following xanthan/sucrose weight ratios: ♦, control, 0; ■, 0.0001; ▲, 0.0005; ○, 0.001; ×, 0.002; ●, 0.004; □, 0.005; and +, 0.01.

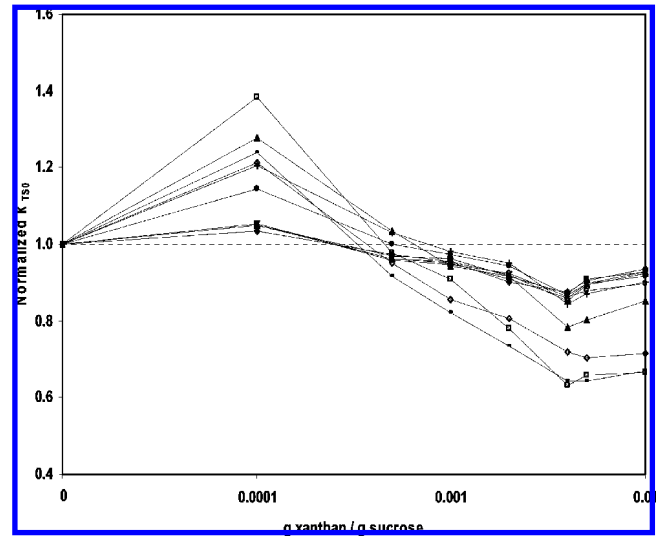

Figure 5. Effect of xanthan content on the rate constant for nonradiative decay of the triplet state (k_{TS0}), normalized at each temperature to the value in pure sucrose. Data were collected at 5 (♦), 15 (■), 25 (△), 35 (×), 45 (○), 55 (●), 65 (+), 75 (▲), 85 (◊), 95 (−), and 100 °C (□).

at high temperature, β was higher in the presence of xanthan. Because β sensitively reflects the width of the distribution of Ery B lifetimes (*14*), and thus the corresponding distribution of dynamically distinct probe environments with different values of k_{TS0} (*10*), the small increase in β reflected a significant decrease in the range of dynamically distinct probe environments both at low temperature (except at weight ratio of 0.01) and at high temperature (except at weight ratio of 0.0001).

The decrease in lifetime with temperature reflects an increase in the rate of nonradiative decay of the excited triplet state T_1 due to an increase in both the rate of nonradiative decay to the ground-state S_0 (k_{TS0}) and the rate of reverse intersystem crossing to S_1 (k_{TS1}). On the basis of the maximum physically reasonable value of k_{TS1} (*10*), an estimate of the lower limit of k_{TS0} was calculated from eq 5 (Materials and Methods) and is plotted as $\ln(k_{TS0})$ vs $1/T$ in **Figure 4**. The nonradiative quenching rate k_{TS0} was essentially constant at low temperature and increased dramatically at higher temperature; the increase occurred at ~60 °C in pure sucrose, indicating that k_{TS0} is sensitive to molecular mobility activated at the glass transition (*10*). In general, the addition of xanthan decreased the quenching rate k_{TS0} over the entire temperature range in a dose-dependent manner; the decrease was more significant at higher temperature. The addition of low concentrations of xanthan (weight ratio 0.0001), however, increased the quenching rate k_{TS0} over the entire temperature range; this increase was slight at low and more dramatic at high temperatures. The transition temperatures, calculated from the intersection of linear fits to low and high temperature data, were estimated as 76.5 °C for sucrose and 72.7, 76.9, 81.4, 80.9, 80.4, 85.2, and 86.2 °C for xanthan weight ratios of 0.0001, 0.0005, 0.001, 0.002, 0.004, 0.005, and 0.01, respectively. As compared with sucrose, the transition temperature decreased at low (weight ratio 0.0001), increased slightly at intermediate (0.001−0.004), and increased significantly at high xanthan contents (≥0.005).

The variation of k_{TS0} with xanthan content is plotted in **Figure 5** where k_{TS0} is normalized to the value in pure sucrose at each temperature. The quenching rate increased above that seen in pure sucrose at a weight ratio of 0.0001 and decreased below that seen in sucrose at higher xanthan concentrations; the extent of the increase (at weight ratio 0.0001) and of the decrease (at weight ratio 0.004) increased in magnitude as the temperature increased. The magnitude of k_{TS0} reflects the ability of the excited triplet T_1 state to couple with highly excited vibrations of the singlet S_1 ground state and, more significantly, the ability of the matrix to dissipate these vibrational excitations (*16*). This rate is sensitive to the molecular mobility of the amorphous matrix in which the probe is embedded (*10*).

Spectral Heterogeneity. Phosphorescence intensity decays of Ery B were measured as a function of excitation and emission wavelengths at 25 °C in sucrose films with different xanthan contents. All decays were well-analyzed using a stretched exponential decay model. The quenching rates k_{TS0} calculated from the fit lifetimes are plotted vs emission and excitation wavelengths at various xanthan contents in **Figure 6a**. The value of k_{TS0} increased monotonically with increasing emission wavelength in all of the films. At low xanthan content (weight ratio 0.0001) k_{TS0} was above, and at higher xanthan contents (≥0.0005), k_{TS0} was below that seen in pure sucrose at all emission wavelengths. The variation of k_{TS0} was quantified using the difference in k_{TS0} across the emission band (Δk_{TS0}). The value of Δk_{TS0} decreased below the value in pure sucrose in all xanthan−sucrose films except for films with a weight ratio of 0.01, where k_{TS0} increased by ~10%. Across the excitation band, k_{TS0} exhibited a minimum at ~530 nm and had higher values at both the blue and the red edge of the excitation band in all sucrose and sucrose−xanthan films.

The stretching exponent β also varied as a function of both excitation and emission wavelength (**Figure 6b**). In all films, β values were lower at the blue edge in both emission and excitation bands, increased with increasing wavelength to a maximum at 680−690 nm in the emission band and a maximum at 540−550 nm in the excitation band, and then decreased slightly at the red edge. The values of β were generally higher in the presence of xanthan, except at a weight ratio of 0.01. The variation of β across the emission as well as excitation band in sucrose films was generally smaller in the presence of xanthan. At the high end of the xanthan content (weight ratio of 0.01), the values of β were lower, but the variation of β was larger than in pure sucrose.

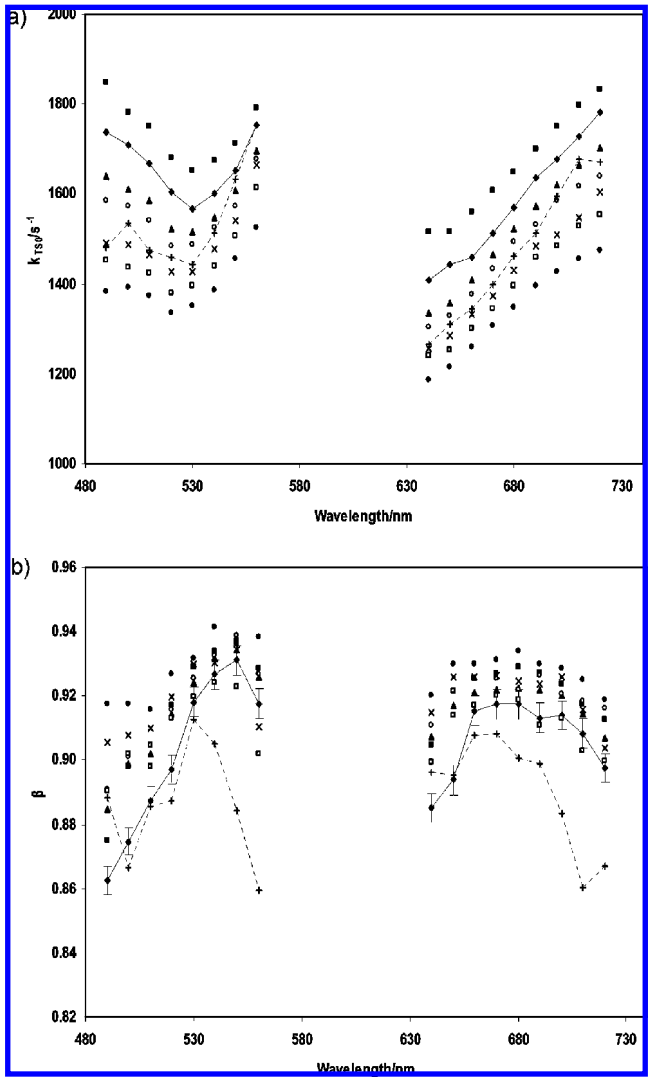

Figure 6. Effect of excitation wavelength (with 680 nm emission) and emission wavelength (with 530 nm excitation) on the nonradiative decay rate k_{TS0} (**a**) and stretching exponent β (**b**). Data are from fits of Ery B phosphorescence intensity decays to the stretched exponential decay model at the following xanthan/sucrose weight ratios: ♦, control, 0; ■, 0.0001; ▲, 0.0005; ○, 0.001; ×, 0.002; ●, 0.004; □, 0.005; and +, 0.01.

DISCUSSION

The shape of the Ery B emission spectra collected from sucrose−xanthan mixtures was identical to that seen in pure sucrose, indicating that the probe molecules did not aggregate with the addition of xanthan. The phosphorescence characteristics of the probe thus report on the physical properties of the local matrix environment.

Matrix Molecular Mobility. The phosphorescence peak frequency reflects the average extent of dipolar relaxation occurring around the excited probe during the triplet state lifetime; it thus reflects a balance between the rate of dipolar relaxation and the rate (lifetime) of emission (*17*). Because the probe lifetime decreased at low and increased at high xanthan contents, the systematic variation of the peak frequency indicates that the dipolar relaxation rate increased at low (∼0.0001 weight ratio) and decreased at high (0.001−0.01 weight ratio) levels of xanthan as compared to the rate in pure sucrose, with the changeover occurring at a weight ratio of ∼0.0005. In amorphous solid sugars, dipolar relaxation reflects mobility of the hydroxyl groups of sugars due to localized β-relaxations in the glass or to large-scale α-relaxations associated with flow activated at T_g. The presence of a very small amount of xanthan thus increases the rate at which these hydroxyl groups can reorient around the excited probe, while a higher level of xanthan decreases the rate of hydroxyl group reorientation.

The rate of intersystem crossing k_{TS0} reflects both the extent to which the excited T_1 state is vibrational coupled to the S_0 ground state as well as the rate at which the highly excited ground-state vibrational energy can dissipate from the probe into the surrounding matrix. The efficiency of this vibrational dissipation is related to the overall mobility of the matrix; k_{TS0} thus provides a direct measure of matrix mobility, which we refer to as the rate of matrix collisional quenching. The effect of xanthan content on k_{TS0} was identical to that seen for dipolar relaxation: This rate increased at a weight ratio of 0.0001 and decreased at weight ratios of 0.001−0.01, with the changeover occurring at a weight ratio of ∼0.0005.

The presence of a very small amount of xanthan thus appeared to increase both the rate of dipolar relaxation and the rate of collisional quenching, and the presence of larger xanthan concentrations decreased both of these rates; the changeover from increasing to decreasing mobility of the sucrose matrix occurred at a weight ratio ∼0.0005 for both measures of matrix mobility.

Matrix Dynamic Site Heterogeneity. Supercooled liquids and amorphous polymers are dynamically heterogeneous (*18*). Spectral heterogeneity consistent with such dynamic heterogeneity is observed when Ery B is dispersed in amorphous sugars and sugar alcohols (*12*) and in proteins (*19*), indicating that dynamic site heterogeneity may be a characteristic feature of amorphous biomaterials. Pravinata et al. (*10*) proposed a physical model for the origin of this spectral heterogeneity in which probes are distributed among matrix sites that differ in molecular mobility; those probes in local environments with less-constrained packing have a higher overall molecular mobility (and thus shorter lifetime) and also faster dipolar relaxation rate (and thus lower emission energy), while those probes in local environments with more constrained packing have a lower overall molecular mobility (and thus longer lifetime) and also slower dipolar relaxation rate (and thus higher emission energy).

Our study provides three independent spectral measures of matrix dynamic heterogeneity: the width of the emission band, the value of the stretching exponent β, and the variation of k_{TS0} with wavelength. All three measures indicate that the addition of xanthan gum decreases the extent of dynamic heterogeneity within the amorphous sucrose matrix.

The emission bandwidth, which reflects the extent of inhomogeneous broadening, decreased slightly with xanthan addition, indicating a decrease in the width of the distribution of energetically distinct matrix environments; interestingly, the largest decrease was seen at a weight ratio 0.0001. The stretching exponent β provides a measure of the width of the distribution of lifetimes required to fit the phosphorescence emission transients (*10*), with smaller values indicating a broader distribution (*14*); the distribution of lifetimes in turn reflects variations in k_{TS0} due to the presence of a distribution of sites with different molecular mobility (*10*). The values of β increased in general with the addition of xanthan, suggesting that xanthan decreased the extent of matrix dynamic heterogeneity. Finally, the addition of xanthan gum, except at a weight ratio of 0.01, also decreased the total variation of quenching rate k_{TS0} with emission wavelength at 25 °C. This decrease also suggests that xanthan decreased the extent of dynamic heterogeneity in amorphous sucrose.

Interactions between Xanthan Gum and Sucrose. Xanthan gum, essentially modified cellulose, is composed of 1,4-linked β-glucopyranose residues modified at the 3-position of, on average, alternating residues with the trisaccharide β-D-Man*p*-(1→4)-β-D-Glc*p*A-(1→2)-α-D-Man*p*; the initial mannose is acetylated at position 6, and about 50% of the terminal mannose residues are ketalized with pyruvate at positions 4 and 6 (*20*). The polymer is relatively stiff; how stiff is uncertain as the measured persistence length varies from 40 nm (*21*) to over 400 nm (*22*), depending upon conditions and measurement techniques. The behavior of xanthan in solution is complicated by changes in conformation and by self-association; although the conformation is clearly helical at low temperature and undergoes a helix−coil transition to a random coil at higher temperature, there is a long-standing controversy about whether the low temperature conformation is a single or a double helix (*23*). The helix−coil transition temperature is sensitive to ionic strength, with transition temperatures ranging from ∼10 to 70 °C over the ionic strength range from ∼1 to 100 mM (*24*). There do not appear to be any studies of the effect of sucrose on xanthan stiffness or conformation. Although xanthan shows weak gel properties under some conditions at high concentrations, it is considered a nongelling hydrocolloid (*25*).

Differential scanning calorimetry measurements show that xanthan and other hydrocolloids do not influence the T_g and thermal properties of sucrose solutions at subzero temperatures (*26*). The T_g of sucrose−xanthan mixtures was estimated using the Couchman and Karasz equation (eq 3) and a xanthan T_g = 212 °C [calculated based on chemical structure and additive group contributions using van Krevelen's method (*27*)]. At the xanthan levels used in this study, the calculated T_g values of sucrose were not significantly influenced. Although the transition temperatures calculated from the Arrhenius plots of k_{TS0} increased slightly with xanthan content, the maximum change in transition temperature was only ∼11 °C (although the transition temperature actually decreased at a weight ratio of 0.0001). The presence of xanthan just barely increased the amount of residual water in the films, from 0.56 ± 0.13 weight % in pure sucrose to 0.72 ± 0.21 weight % at a 0.01 weight ratio xanthan (further data are itemized in the Materials and Methods), with no systematic changes reflective of the complex variations in matrix mobility monitored here. It thus appears that the effects of xanthan on sucrose molecular mobility reflect complex, specific interactions between xanthan and sucrose rather than merely a bulk effect of the polymer on the matrix glass transition temperature.

Undoubtedly, the specific xanthan conformation could affect the properties of the sucrose matrix. Heat treatment of xanthan solutions denatured the ordered xanthan structure (*28*). Xanthan-containing solutions were thus uniformly heat treated to 60 °C before rapid film casting and drying; given that film-forming solutions contained no salt, a condition that both favors unfolding and lowers the xanthan helix−coil transition temperature, this temperature should be sufficient to ensure that xanthan molecules are in a uniformly disordered structure within the sucrose matrix.

The concentration at which xanthan polymer chains begin to overlap in aqueous solution (C^*) is in the range from 0.00013 to 0.00025 g/mL (*23*). These values are comparable to, albeit slightly smaller than, the weight ratio for the dynamic changeover discussed above, suggesting that the observed crossover from a low weight ratio where xanthan increases matrix mobility to a high weight ratio where xanthan decreases matrix mobility actually reflects the changeover from a low concentration regime where xanthan polymer chains are dispersed individually throughout the sucrose matrix to a high concentration regime where chains begin to overlap and entangle one another. This argument is further supported by a similar dose-dependent effect on sucrose matrix mobility seen in hot-cast gelatin−sucrose films (*9*). In the gelatin-containing films, the crossover from increasing to decreasing matrix mobility occurred at ∼0.003 weight ratio gelatin, in excellent agreement with the chain overlap concentration of ∼0.0035 g/mL seen in aqueous solutions of gelatin in the random coil conformation (*29*).

Molecular dynamics simulations at zero or low water content indicate that sucrose molecules form extended hydrogen-bonded clusters separated by connected regions of free volume (*30*). We thus speculate that the presence of xanthan, with its different ability to form hydrogen bonds and the extensive constraints placed on its sugar residue conformational freedom by the polymeric structure, may disrupt the hydrogen-bonded network of the pure sucrose matrix, thus disrupting sucrose clusters and consequently increasing matrix mobility. At higher xanthan contents, the presence of chain entanglements and xanthan−xanthan interactions throughout the matrix may generate a polymeric (covalent) cluster network that consequently decreases matrix mobility.

These data indicate that the addition of xanthan gum to an amorphous sucrose matrix has complex, dose-dependent effects on the molecular mobility of the amorphous sucrose matrix. Presumably because of the high molecular mass (up to several million Daltons) and large persistence length of xanthan, this polymer has dynamic effects on the sucrose matrix at concentrations as low as a 0.0001 weight ratio. Given the relationship between the molecular mobility and the rates of chemical reaction and physical change in amorphous solids, an increase in molecular mobility at low levels of xanthan gum may actually destabilize the amorphous matrix. The decrease in mobility at higher xanthan contents may, thus, for the same reasons, stabilize the amorphous matrix. Intriguing similarities between the changeover concentration seen in this study and the critical concentration for chain overlap in solution suggest that the dynamic effects of xanthan on amorphous sucrose (and perhaps other amorphous sugars) reflect a similar phenomenon. When interpreted in light of what is known from molecular dynamics about the structure of the amorphous sucrose matrix, xanthan at low concentration may increase molecular mobility by disrupting the local hydrogen-bonded network built up among sucrose molecules, while at a high concentration xanthan may decrease the molecular mobility by providing a stronger, covalently bonded polymer network. Consequently, both of these effects should be taken into consideration during the use of xanthan (and perhaps other biopolymers) in solid solutions of sugars.

Dynamic site heterogeneities above and below the glass transition temperature appear to be a characteristic feature of amorphous food and biomaterials. Although the functional consequences of such dynamic heterogeneity in amorphous biomaterials are unclear, these data indicate that an increase in compositional heterogeneity upon the addition of xanthan gum to sucrose actually results in a decrease in dynamic heterogeneity. Clearly, much remains uncertain about how composition modulates the local structure and dynamics of amorphous solid foods and biomaterials.

LITERATURE CITED

(1) Le Meste, M.; Champion, D.; Roudaut, G.; Blond, G.; Simatos, D. Glass transition and food technology: A critical appraisal. *J. Food Sci.* **2002**, *67*, 2444–2458.

(2) Craig, D. Q.; Royall, P. G.; Kett, V. L.; Hopton, M. L. The relevance of the amorphous state to pharmaceutical dosage forms: Glassy drugs and freeze-dried systems. *Int. J. Pharm.* **1999**, *179*, 179–207.
(3) Crowe, J. H.; Carpenter, J. F.; Crowe, L. M. The role of vitrification in anhydrobiosis. *Annu. Rev. Physiol.* **1998**, *60*, 73–103.
(4) Chang, L.; Shepherd, D.; Sun, J.; Ouellette, D.; Grant, K. L.; Tang, X.; Pikal, M. J. Mechanisms of protein stabilization by sugars during freeze-drying and storage: Native structure preservation, specific interaction, and/or immobilization in a glassy matrix. *J. Pharm. Sci.* **2005**, *94*, 1427–1444.
(5) Franks, F.; Hatley, R. H. M.; Mathias, S. F. Materials science and the production of shelf-stable biologicals. *BioPharm.* **1991**, *4*, 38, 40−42, 55.
(6) Crowe, J. H.; Crowe, L. M.; Carpenter, J. F. Preserving dry biomaterials: the water replacement hypothesis. Part 1. *BioPharm.* **1993**, *6*, 28−29, 32−33.
(7) You, Y.; Ludescher, R. D. The effect of NaCl on matrix mobility in amorphous sucrose detected by phosphorescence from the triplet probe erythrosin B. *Carbohydr. Res.* **2008**, *343*, 350–363.
(8) You, Y.; Ludescher, R. D. The effect of salts on molecular mobility in amorphous sucrose from erythrosin B phosphorescence. *Carbohydr. Res.* **2008**, *343*, 2641–2649.
(9) You, Y.; Ludescher, R. D. Effect of gelatin on molecular mobility in amorphous sucrose detected by erythrosin B phosphorescence. *Carbohydr. Res.* **2008**, *343*, 2657–2666.
(10) Pravinata, L. C.; You, Y.; Ludescher, R. D. Erythrosin B phosphorescence monitors molecular mobility and dynamic site heterogeneity in amorphous sucrose. *Biophys. J.* **2005**, *88*, 3551–3561.
(11) You, Y.; Ludescher, R. D. Phosphorescence of erythrosin B as a robust probe of molecular mobility in amorphous solid sucrose. *Appl. Spectrosc.* **2006**, *60*, 813–819.
(12) Shirke, S.; You, Y.; Ludescher, R. D. Molecular mobility and dynamic site heterogeneity in amorphous lactose and lactitol from erythrosin B phosphorescence. *Biophys. Chem.* **2006**, *123*, 122–133.
(13) Maroncelli, M.; Fleming, G. R. Picosecond solvation dynamics of coumarin 153: The importance of molecular aspects of solvation. *J. Chem. Phys.* **1987**, *86*, 6221–6239.
(14) Lindsey, C. P.; Patterson, G. D. Detailed comparison of the Williams-Watts and Cole-Davidson functions. *J. Chem. Phys.* **1980**, *73*, 3348–3357.
(15) Duchowicz, R.; Ferrer, M. L.; Acuna, A. U. Kinetic spectroscopy of erythrosin phosphorescence and delayed fluorescence in aqueous solution at room temperature. *Photochem. Photobiol.* **1998**, *68*, 494–501.
(16) Papp, S.; Vanderkooi, J. M. Tryptophan phosphorescence at room temperature as a tool to study protein structure and dynamics. *Photochem. Photobiol.* **1989**, *49*, 775–784.
(17) Lakowicz, J. R. In *Principles of Fluorescence Spectroscopy*, 3rd ed.; Lakowicz, J. R., Ed.; Springer: New York, 2006.
(18) Ediger, M. D. Spatially heterogeneous dynamics in supercooled liquids. *Annu. Rev. Phys. Chem.* **2000**, *51*, 99–128.
(19) Lukasik, K. V.; Ludescher, R. D. Effect of plasticizer on dynamic site heterogeneity in cold-cast gelatin films. *Food Hydrocolloids* **2006**, *20*, 88–95.
(20) Belitz, H. D.; Grosch, W.; Schieberle, P. Carbohydrates. In *Food Chemistry*, 3rd ed.; Springer: Berlin, Germany, 2004; p 333.
(21) Chazeau, L.; Milas, M.; Rinaudo, M. Conformers of xanthan in solution: analysis by steric exclusion chromatography. *Int. J. Polym. Anal. Charact.* **1995**, *2*, 21–29.
(22) Camesano, T. A.; Wilkinson, K. J. Single molecule study of xanthan conformation using atomic force microscopy. *Biomacromolecules* **2001**, *2*, 1184–1191.
(23) Viebke, C. Order-disorder conformational transition of xanthan gum. In *Polysaccharides: Structural Diversity and Functional Versatility*; Dumitriu, S., Ed.; Marcel Dekker: New York, 2005; pp 459−474.
(24) Milas, M.; Rinaudo, M. Conformational investigation on the bacterial polysaccharide xanthan. *Carbohydr. Res.* **1979**, *76*, 189–196.
(25) Giannouli, P.; Morris, E. R. Cryogelation of xanthan. *Food Hydrocolloids* **2003**, *17*, 495–501.
(26) Goff, H. D.; Caldwell, K. B.; Stanley, D. W.; Maurice, T. J. The influence of polysaccharides on the glass transition in frozen sucrose solutions and ice cream. *J. Dairy Sci.* **1993**, *76*, 1268–1277.
(27) Khachatoorian, R.; Petrisor, I. G.; Yen, T. F. Prediction of plugging effect of biopolymers using their glass transition temperatures. *J. Pet. Sci. Eng.* **2004**, *41*, 243–251.
(28) Milas, M.; Reed, W. F.; Printz, S. Conformation and flexibility of native and re-natured xanthan in aqueous solutions. *Int. J. Biol. Macromol* **1996**, *18*, 211–221.
(29) Guo, L.; Colby, R. H.; Lusignan, C. P.; Whitesides, T. H. Kinetics of triple helix formation in semidilute gelatin solutions. *Macromolecules* **2003**, *36*, 9999–10008.
(30) Molinero, V.; Cagin, T.; Goddard, W. A., III. Sugar, water and free volume networks in concentrated sucrose solutions. *Chem. Phys. Lett.* **2003**, *377*, 469–474.

Received for review August 12, 2008. Revised manuscript received November 13, 2008. Accepted November 24, 2008. This research was partially supported by funds provided by the CSREES of the U.S. Department of Agriculture, Grant 2002-01585.

JF802501M